JOURNAL OF GUIDANCE, CONTROL, AND DYNAMICS
Vol. 38, No. 4, April 2015

Stability of Spinning Satellite Under Axial Thrust, Internal Mass Motion, and Damping

Frank L. Janssens*
2201 KA Noordwijk, The Netherlands
and
Jozef C. van der Ha†
Deming, Washington 98244

DOI: 10.2514/1.G000123

The paper extends and clarifies the stability results for a spinning satellite under axial thrust in the presence of internal damped mass motion. It is known that prolate and oblate satellite configurations can be stabilized by damped mass motion. Here, the stability boundaries are established by exploiting the properties of the complex characteristic equation and the results are interpreted in terms of the physical system parameters. When the thrust level is the only free parameter, both prolate and oblate satellites can be stabilized provided that the thrust is within a specified range. This result is in contrast to the well-known maximum-axis rule for a free spinner where damping is always stabilizing (destabilizing) for an oblate (prolate) satellite. When adding a suitable spring-mass system, the minimum value of the spring constant that stabilizes the configuration can be established. In practice, however, the damping may well be too weak to be effective. Numerical illustrations are presented for the actual parameters of the Ulysses prolate configuration at orbit injection as well as for a fictitious oblate system. Finally, a new derivation of a previously established first integral for the undamped system is offered and its properties as a Lyapunov function are discussed.

I. Introduction

IN A previous paper [1], the authors investigated the stability of a spinning body under axial thrust and augmented it with a mass-spring system. The point mass is nominally located on the spin axis and can move in a plane perpendicular to the spin axis but is restrained by the spring. This model was proposed by Mingori and Yam [2] for understanding the instability that occurred during the firing of apogee boost motors, where slag could accumulate in an imbedded nozzle. They analyze the stability of this system by using the linearized equations (Lyapunov direct method) about the reference motion consisting of a uniformly spinning system, with the mass particle located on the spin axis. Furthermore, they obtain a stability diagram [2] in terms of two nondimensional parameters, that contains an oscillatory stable and an unstable region. More recently [1], the region of oscillatory stability has been interpreted in terms of the physical parameters. However, the *oscillatory* stability of the linearized system does not assure the stability of the original nonlinear system.

Subsequent studies have added damping to this mass-spring system. Halsmer and Mingori [3] use Lyapunov's second or indirect method by constructing a Lyapunov function, whereas Yam et al. [4] use a special method to evaluate the roots of the characteristic equation with complex coefficients. (Here, we follow the Hughes [5] terminology for Lyapunov methods.) The results show that the region of instability increases dramatically and that part of the remainder of the previously oscillatory stable area turns into a region where the damping guarantees asymptotic stability. This conclusion is valid for both prolate and oblate systems, which contrasts with the familiar maximum-axis rule for a freely spinning body. Therefore, the quoted papers [3,4] no longer interpret the augmented particle as slag but consider the spring-mass-damper system as nutation damper. This approach will also be followed here. It is important to note that the *asymptotic* stability of the linearized system does guarantee the stability of the reference motion for the full nonlinear system [5].

The dynamics presented in this paper holds for any space vehicle that is subjected to an axial thrust force and that has internal damping. In practice, the most relevant applications are for satellites with an attached upper stage or solid rocket motor, and this is the configuration studied here. The focus is on the most common situation when the particle is located aft of the system c.m. The paper investigates the stability of the linearized system including damping by analyzing the roots of the characteristic equation as in Yam et al. [4]. The characteristic equation is written as a polynomial of order three with complex coefficients. In this form, the Routh–Hurwitz or Lienard–Chipart stability theorems cannot be used because they apply only to equations with real coefficients. Gantmacher [6] offers a generalization for equations with complex coefficients, but not all conditions required by this theorem are satisfied here.

Yam et al. [4] discuss the appearance and disappearance of the negative real parts of the roots by a special perturbation method with complex coefficients. Our approach starts by replacing the characteristic equation by an equivalent system of two equations for its real and imaginary parts, respectively. This system contains only real coefficients and has the real σ and imaginary ω parts of the complex variable $p = \sigma + j\omega$ as real variables. The two equations are considered as polynomials in σ with coefficients containing the system parameters and ω. These equations allow zero solutions in σ when their constant terms vanish. The two conditions for having $\sigma = 0$ imply that the frequency ω can take only two values, namely, zero and the nutation frequency of the system.

The proposed approach facilitates the straightforward analysis of the sign changes of the real parts of the roots by using a linearization procedure about the solutions $\sigma = 0$ and the two permissible values of ω. In the first case, both ω and σ vanish and the zero solution of the undamped case is recovered. Both admissible ω solutions define families of straight lines in the stability diagram that separate the solutions $\sigma > 0$ and $\sigma < 0$. The combination of these results leads to an open triangular area between the two straight lines, where all σ values are negative in the prolate case. In the oblate case, however, this area may have a different shape because of the condition that the thrust must be positive. The ensuing asymptotically stable domain confirms and clarifies previous results [3,4].

Presented as Paper AAS 2013-214 at the 23rd AAS/AIAA Space Flight Mechanics Meeting, Kauai, HI, 10–14 February 2013; received 30 June 2013; revision received 5 February 2014; accepted for publication 11 February 2014; published online 2 June 2014.

*Consultant, Wilhelminastraat 29; f.janssens@ziggo.nl.
†Consultant, 5808 Bell Creek Road; jvdha@aol.com. Senior Member AIAA.

The qualitative conclusions established by Halsmer and Mingori [3] for a prolate spinner are confirmed and extended further. In particular, the minimum value of the spring constant that achieves stability is associated with a specific minimum thrust level. For larger values of the spring constant, the minimum thrust level remains unchanged, whereas the maximum thrust value depends on the selected spring constant.

Similar explicit boundary values are also established for an oblate system. The condition for $\sigma < 0$ on the nutation frequency defines now the maximum value of the thrust level. However, the condition that the thrust must be positive eliminates a part of the open triangular stable domain.

These results highlight the severe impact of the axial thrust on the stability conditions in comparison with a free spinner. The physical values of the particle mass, spring constant, and damping coefficient that guarantee asymptotic stability can readily be identified for a given situation. The paper illustrates this for an example based on the Ulysses parameters with a fixed thrust level and a range of particle mass values.

Parametric analyses of the roots show that there always exists one root (i.e., $|\omega| \approx 2\Omega_{\text{spin}}$) that has always a negative σ value. The characteristics of the stability region can be adequately described and interpreted in terms of the behavior of the other two roots. These results are relevant for designing an optimal nutation damper. Lang and Halsmer [7] select the particle location such that the two σ values are equal. However, it is not assured that both frequencies have the same effects on the attitude. One of the stability boundaries is most efficient for the (perturbed) nutation frequency, whereas the other is better for the lower frequency (perturbed from zero) that may have more influence on the depointing, which is a consequence of the instability. The relative importance and amplitude of the frequencies must be assessed before the optimal value for the spring constant can be decided upon. In any case, the application of such a nutation damper is only feasible when there is sufficient time for reducing the nutation.

Finally, the paper offers a new derivation of the first integral discovered by Mingori and Yam [2] for the system without damping and discusses its properties as a Lyapunov function.

II. Model and Nomenclature

A. Physical Model

Figure 1 shows the physical model to be used here, which is consistent with previous papers [1–3]. It consists of a symmetric rigid body of constant mass M and principal moments of inertia C (axial) and A_b (transverse). The body has a constant spin rate Ω and is subjected to a thrust F which is assumed to be pointing perfectly

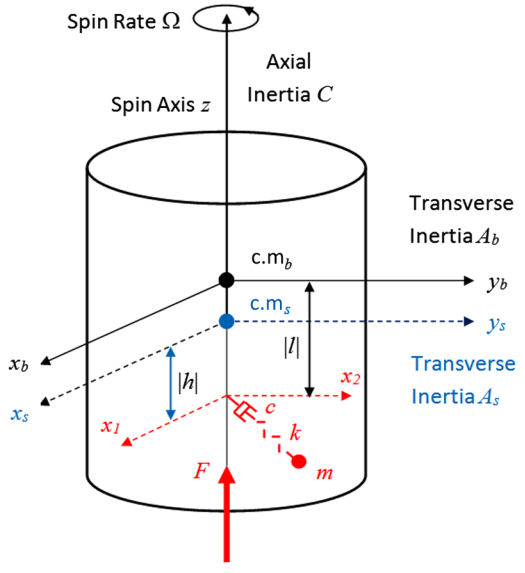

Fig. 1 Model configuration and mass properties.

Table 1 Summary of independent physical and scaling parameters

Parameter	Unit	Description
M	kg	Body mass
C	kg · m^2	Axial moment of inertia (spin inertia)
A_b	kg · m^2	Transverse moment of inertia for axes passing through the body's c.m.$_b$
F	N	Thrust level of rocket motor
Ω	1/s	Spin rate
l	m	Vertical coordinate of particle relative to body c.m.
m	kg	Particle mass
k	kg/s^2	Spring constant or stiffness
c	kg/s	Viscous damping constant
$p_k = A_b\Omega^2/l^2 > 0$	kg/s^2	Scaling parameter for spring constant
$p_c = M\Omega > 0$	kg/s	Scaling parameter for damping constant
$p_{\text{th}} = A_b\Omega^2/\|l\| > 0$	N	Scaling parameter for thrust force
$\delta = Ml^2/A_b = (l/r_g)^2 \geq 0$	— —	Auxiliary parameter; $r_g = (A_b/M)^{1/2}$ is radius of gyration

along the spin axis. The x_b and y_b axes pass through the body's mass center (i.e., c.m.$_b$). Furthermore, the x_s and y_s axes pass through the nominal system mass center c.m.$_b$ when the particle is located in its rest position on the z axis.

Table 1 summarizes the set of independent parameters that appear in the present model. The particle of mass m is nominally located on the spin axis at the distance l from the body's center of mass. For $l > 0$, the particle is on the $+z$ axis and for $l < 0$ it is on the $-z$ axis. The particle may move in an equatorial plane while attached to the spin axis by a linear spring of stiffness k and viscous damping coefficient c. The point of application of the thrust is also taken at l.

The next three rows in Table 1 define the scaling factors for the spring constant ($\sim\Omega^2$), the damping coefficient ($\sim\Omega$), and the thrust force ($\sim\Omega^2$). These positive scaling factors are defined such that they are independent of any of the parameters of the nutation damper by which the satellite is augmented. For consistency, the particle m should be scaled by M but most expressions are simplified when m is scaled by $m + M$. The parameter δ in the final row is the squared ratio of the particle's vertical position l and the radius of gyration r_g of the transverse body inertia. A rough approximation of this ratio may be obtained when replacing r_g by the body radius r (note that $r_g < r$).

B. Derived and Auxiliary Parameters

Table 2 summarizes the derived and auxiliary parameters, which facilitate the translation of the stability results into the relevant physical parameters of the system. Therefore, the physical interpretations of the first nine rows of Table 2 are provided below. All normalization constants are defined as positive.

The first three rows define the system parameters. The total mass of the system is $M + m$ and the associated mass ratios are μ and μ_1. The presence of the particle mass m changes the principal transverse inertia A_b to A_s and the lever arm to the system c.m.$_s$ from l to h. For stability investigations, it turns out that $l < 0$ is the interesting case [1]. The spin inertia C remains unchanged when the particle is on the spin axis and changes only in second order of its distance from the spin axis.

The next row in Table 2 defines the nondimensional independent variable τ. This is followed by the definitions of λ_b, λ_s, and Δ, all of which involve the ratio of the body and the system moments of inertia. Although the numerical differences between (λ_b, λ_s), (A_b, A_s), and (h, l) are small for the present application to a nutation damper (as well as for the slag mass interpretation), it is essential for the proper understanding of the dynamics to make these clear distinctions.

The following three rows define the normalized nondimensional parameters associated with the spring constant k, the damping c, and the thrust F. Next is the resonance frequency ω_{res}^2 of the mass-spring system, normalized by the square of the spin rate. In the dynamic equations, we often encounter the combination $\omega_{\text{res}}^2/\mu_1$. This expresses the fact that the spring does not act between m and a fixed point but between m and the moving mass M. The resonance

Table 2 Summary of auxiliary parameters

Parameter	Unit	Definition	Description
μ, μ_1	— —	$m/(M+m), M/(M+m)$	Ratio relationships between particle mass and total mass
h	m	$\mu_1 l$	Vertical distance of particle to system c.m.$_s$
A_s	kg · m^2	$A_b + \mu_1 m l^2 = A_b + mhl$	Transverse moment of inertia relative to system c.m.$_s$
τ	— —	Ωt	Angular independent variable
$0 \le \lambda_b \le 2$	— —	C/A_b	Precession rate of angular velocity, normalized by the spin rate Ω (note, the nutation frequency is $\lambda_b - 1$)
$0 \le \lambda_s \le 2$	— —	C/A_s	As in the preceding row, but in terms of the system moments of inertia
$\Delta = 1 + \mu\delta$	— —	$A_s/A_b = \lambda_b/\lambda_s$	Ratio of principal system and body transverse inertias
$k_n \ge 0$	— —	k/p_k	Normalized spring constant or stiffness
$c_n \ge 0$	— —	c/p_c	Normalized viscous damping coefficient
f_n	— —	F/p_{th}	Normalized thrust force of rocket motor
ω_{res}^2	— —	$k/(m\Omega^2)$	Resonance frequency of mass-spring system attached to a fixed point, normalized by the spin rate
γ^2, β^2	— —	$\gamma^2 = \omega_{\text{res}}^2/\mu_1, \beta^2 = \gamma^2/\lambda_b^2$	$\Rightarrow \gamma^2 = k_n/(\mu\delta)$
$T_{0\lambda}, T_0$	— —	$T_{0\lambda} = k_n - \mu f_n, T_0 = T_{0\lambda}/\lambda_b^2$	$\Rightarrow A_b\Omega^2 T_{0\lambda} = l^2 k + mlg$ with $g = F/(m+M)$

frequency for such a system depends on an equivalent mass $m_{\text{eq}} = mM/(m+M)$ which leads to the expression $\omega_{\text{res}}^2/\mu_1$.

The last two rows in Table 2 give the definitions of β^2, T_0, which are the nondimensional parameters used in the stability diagram (see also [1]). After multiplication by λ_b^2, they become $\{\gamma^2, T_{0\lambda}\}$.

III. Transverse Dynamics Including Damping

A. Equations of Motion

The derivation of the equations of motion for the dynamic satellite model in Fig. 1 resembles closely Eqs. (1–5) of [1]. The linearized equations of the transverse dynamics about the reference motion are described by the first-order variables $\{\omega_1, \omega_2, x_1, x_2\}$. The rates ω_1, ω_2 are the transverse angular velocity components, normalized by the spin rate Ω, in a body-fixed reference frame. The variables x_1, x_2 are the components of the particle's displacement with respect to the spin axis. When including the additional damping terms (see also Eqs. 1–10 of Yam et al. [4]), the resulting equations of motion for the system are

$$A_s\omega_1' + (C - A_s)\omega_2 = mh\{x_2'' + 2x_1' - x_2\} - (\mu F/\Omega^2)x_2 \quad (1a)$$

$$A_s\omega_2' - (C - A_s)\omega_1 = mh\{-x_1'' + 2x_2' + x_1\} + (\mu F/\Omega^2)x_1 \quad (1b)$$

$$x_1'' - 2x_2' - (1 - \omega_{\text{res}}^2/\mu_1)x_1 + (c_n/\mu)x_1' = -h(\omega_2' + \omega_1)/\mu_1 \quad (1c)$$

$$x_2'' + 2x_1' - (1 - \omega_{\text{res}}^2/\mu_1)x_2 + (c_n/\mu)x_2' = h(\omega_1' - \omega_2)/\mu_1 \quad (1d)$$

The final two equations contain the viscous damping terms, which are expressed in terms of the nondimensional parameter c_n defined in Table 2.

By applying similar transformations and substitutions as were used in Eqs. (1–5) of [1], the following set of equations can be established for the body motion:

$$\omega_1' + (\lambda_b - 1)\omega_2 + (T_{0\lambda}x_2 + c_n\delta x_2')/l = 0 \quad (2a)$$

$$\omega_2' - (\lambda_b - 1)\omega_1 - (T_{0\lambda}x_1 + c_n\delta x_1')/l = 0 \quad (2b)$$

$$x_1'' - 2x_2' + (T_{0\lambda} + \gamma^2 - 1)x_1 + (c_n\Delta/\mu)x_1' + l\lambda_b\omega_1 = 0 \quad (2c)$$

$$x_2'' + 2x_1' + (T_{0\lambda} + \gamma^2 - 1)x_2 + (c_n\Delta/\mu)x_2' + l\lambda_b\omega_2 = 0 \quad (2d)$$

where (see Tables 1 and 2)

$$c_n = \frac{c}{M\Omega} \quad (3a)$$

$$\delta = \frac{Ml^2}{A_b} \quad (3b)$$

$$\Delta = 1 + \mu\delta \quad (3c)$$

The sixth-order system in Eqs. (2) is suitable for stability analyses even though it contains no information on the body's attitude motion. The attitude orientation may be included by introducing two additional equations for the small attitude angles $\{\theta_1, \theta_2\}$ in terms of the rates $\omega_i (i = 1, 2)$.

After introducing the complex variables $\omega_c = \omega_1 + j\omega_2$ and $x_c = x_1 + jx_2$, we can write Eqs. (2) as

$$\omega_c' - j(\lambda_b - 1)\omega_c - j(T_{0\lambda}x_c + c_n\delta x_c')/l = 0 \quad (4a)$$

$$x_c'' + (c_n\Delta/\mu + 2j)x_c' + (T_{0\lambda} + \gamma^2 - 1)x_c + l\lambda_b\omega_c = 0 \quad (4b)$$

An important advantage of employing a formulation in terms of complex variables is because the corresponding characteristic equation has order three instead of six because each of its solutions has multiplicity two in the original system of Eqs. (2).

B. Characteristic Equation

To investigate the stability of the linear system in Eqs. (4), we use the "ansatz" $\exp(p\tau)$ for the solutions $\omega_c(\tau)$ and $x_c(\tau)$ of Eqs. (4). This leads to the dynamic stiffness matrix $Z(p)$, whose determinant equals the characteristic equation $D(p)$ of the system in Eqs. (4):

$$D(p) = \text{Det}[Z(p)] = \text{Det}\begin{bmatrix} p - j(\lambda_b - 1) & -j(T_{0\lambda} + c_n\delta p)/l \\ l\lambda_b & p^2 + (c_n\Delta/\mu + 2j)p + T_{0\lambda} + \gamma^2 - 1 \end{bmatrix} = 0 \quad (5)$$

The function $D(p)$ is a third-degree polynomial of the variable $p = \sigma + j\omega$ and can be expressed as

$$D(p) = p^3 + a_2p^2 + a_1p + a_0 = 0 \quad (6)$$

Next, the coefficients in Eq. (6) are split up explicitly in their real and imaginary parts:

$$a_2 = a_{2r} + ja_{2i} \quad (7a)$$

$$\text{with} \quad a_{2r} = c_n\Delta/\mu \tag{7b}$$

$$a_{2i} = 3 - \lambda_b \tag{7c}$$

$$a_1 = a_{1r} + ja_{1i} \tag{8a}$$

$$\text{with} \quad a_{1r} = T_{0\lambda} + \gamma^2 + 2\lambda_b - 3 \tag{8b}$$

$$a_{1i} = c_n(\Delta - \lambda_b)/\mu \tag{8c}$$

$$a_0 = 0 + ja_{0i} \tag{9a}$$

$$\text{with} \quad a_{0i} = T_{0\lambda} - (\lambda_b - 1)(\gamma^2 - 1) \tag{9b}$$

The condition for the existence of constant (i.e., zero frequency $p = 0$) solutions of the system in Eqs. (4) is satisfied if the coefficient a_{0i} in Eq. (9b) vanishes. This condition is identical to Eq. (19b) of [1], which confirms that the condition for constant solutions does not depend on the damping coefficient and remains valid in the presence of damping (i.e., when $c_n \neq 0$).

In the absence of damping, the parameter c_n vanishes and the coefficient a_2 (in addition to a_0) is purely imaginary, whereas a_1 is purely real. After changing the variable p into $p_1 = jp = -\omega + j\sigma$, all coefficients $a_j (j = 0, 1, 2)$ of $D(p_1)$ in Eq. (6) become real and the associated solutions are oscillatory stable. Thus, the stability condition is satisfied if all roots of $D(p_1) = 0$ are real. This result is already known from Eq. (26) and the following text in [1].

The expressions in Eqs. (6–9) show that, in general, the coefficients $a_j (j = 0, 1, 2)$ of the polynomial $D(p)$ in Eq. (6) are complex. The Routh–Hurwitz theorem holds only for equations with real coefficients and can thus not be used for the present third-order formulation. (For a sixth-order system, the application of the Routh–Hurwitz theorem becomes too complicated [3].) Gantmacher [6] presents a generalization of the Routh–Hurwitz theorem for a system with complex coefficients but, unfortunately, not all conditions of his theorem are satisfied in the present case. Therefore, a different novel approach is proposed here. The properties of the roots of the characteristic equation $D(p)$ are evaluated by studying an equivalent system of equations with real coefficients in the real variables σ and ω.

The complex characteristic equation $D(p) = 0$ in Eq. (6) is split up (by writing $p = \sigma + j\omega$) into two polynomial equations for its real and imaginary parts, which contain only real variables:

$$\mathrm{Re}\{D(p)\} = \sigma^3 + a_{2r}\sigma^2 + b_{1r}\sigma + b_{0r} = 0 \tag{10a}$$

$$\mathrm{Im}\{D(p)\} = b_{2i}\sigma^2 + b_{1i}\sigma + b_{0i} = 0 \tag{10b}$$

with

$$b_{1r} = T_{0\lambda} + \gamma^2 + (1 + \omega)\{2\lambda_b - 3(1 + \omega)\} \tag{11a}$$

$$b_{0r} = -c_n\omega\Delta(1 + \omega - \lambda_s)/\mu \tag{11b}$$

$$b_{2i} = 3(1 + \omega) - \lambda_b \tag{12a}$$

$$b_{1i} = c_n\Delta(1 + 2\omega - \lambda_s)/\mu \tag{12b}$$

$$b_{0i} = (1 + \omega)T_{0\lambda} + (1 + \omega - \lambda_b)\{\gamma^2 - (1 + \omega)^2\} \tag{12c}$$

It may be noted that $\Delta = \lambda_b/\lambda_s$ (with $\lambda_b > \lambda_s$) clarifies the physical interpretation of the parameter Δ, which has also been used by Yam et al. [4].

IV. Stability Investigations

A. Stability in Absence of Damping

In the absence of damping, the parameter $c_n = 0$ so that the coefficients a_{2r}, b_{0r}, and b_{1i} vanish according to Eqs. (7b), (11b), and (12b). Therefore, Eq. (10a) is reduced to

$$\mathrm{Re}\{D(p)\} = (\sigma^2 + b_{1r})\sigma = 0 \tag{13a}$$

$$\Rightarrow \sigma = 0 \tag{13b}$$

$$\text{or} \quad \sigma^2 = -b_{1r} \tag{13c}$$

1. Case $\sigma = 0$

These are the solutions with oscillatory stability. Because of the condition in Eq. (10b), they can only exist if also

$$\mathrm{Im}\{D(p)\} = b_{2i}\sigma^2 + b_{0i} = 0 \tag{14a}$$

$$\Rightarrow b_{0i} = \omega_1 T_{0\lambda} - (\lambda_b - \omega_1)(\gamma^2 - \omega_1^2) = 0 \tag{14b}$$

where $\omega_1 = 1 + \omega$. For vanishing ω, Eq. (14b) reproduces the relationship $T_{0\lambda}(\gamma^2)$ for the constant solutions, see Eq. (19b) of [1].

The condition for oscillatory stability requires that all three roots ω_j $(j = 1, 2, 3)$ of the third-order polynomial in Eq. (14b) must be real. This is due to the fact that complex roots occur always in conjugate pairs and their imaginary parts are in fact σ values in the original variable p. The one root of the pair that has the positive imaginary part leads to an instability. The equation that expresses this condition produces the stability curve (in the absence of damping) that was established in Eqs. (27) of [1].

2. Case $\sigma^2 = -b_{1r}$

Under this condition, the two roots are

$$\sigma_{2,3} = \pm\sqrt{-b_{1r}} \tag{15}$$

As long as $b_{1r} < 0$ is satisfied, both solutions $\sigma_{2,3}$ are real. Obviously, the positive root σ_2 leads to instability in this case.

B. Stability in Presence of Damping

In the general case, damping is present and the parameter $c_n \neq 0$. Equation (6) shows that constant solutions $p = 0$ (i.e., $\sigma = \omega = 0$) exist in the particular case when a_0 vanishes. Equation (9b) indicates that a_0 contains only an imaginary part so that

$$a_{0i} = T_{0\lambda} - (\lambda_b - 1)(\gamma^2 - 1) = 0 \tag{16}$$

This is the condition for the existence of constant solutions that was established and interpreted in Eq. (19b) of [1]. It is important to recognize that Eq. (16) provides only a *sufficient* condition for $\sigma = 0$. The *necessary and sufficient* conditions are given by Eqs. (11b) and (12c):

$$b_{0r} = b_{0i} = 0 \tag{17}$$

The first part of Eq. (17) leads to the following conditions [see Eq. (11b)]:

$$b_{0r} = -c_n\omega\Delta(1 + \omega - \lambda_s)/\mu = 0 \tag{18a}$$

$$\Rightarrow \omega = 0 \tag{18b}$$

$$\text{or} \quad \omega = \lambda_s - 1 \tag{18c}$$

where $\lambda_s = \lambda_b/\Delta$ and $\lambda_s < 1$ is a prolate system. The fact that $\sigma = 0$ can only be achieved when ω takes one of the two values specified in Eqs. (18b) and (18c) is a remarkable result. It offers the possibility to analyze the sign of σ (which defines the stability) in the neighborhood of the ω values in Eqs. (18b) and (18c) and $\sigma = 0$ by using a straightforward linearization procedure. The first-order deviations from the reference values $\sigma = 0$ and $\omega = 0$ (or $\omega = \lambda_s - 1$, respectively) are denoted by $\delta\sigma$ and $\delta\omega$.

The linear equations in $\delta\sigma$ and $\delta\omega$ can readily be derived from Eqs. (10a) and (10b). Because the reference value of σ vanishes, only the constant and linear terms in σ need to be considered. The four coefficients $b_{jk}(j = 0, 1; k = r, i)$ contain the variable ω, which must now be replaced by $\omega_{\text{ref}} + \delta\omega$ (where ω_{ref} stands for either zero or $\lambda_s - 1$). The coefficients of $\delta\sigma$ in Eqs. (10a) and (10b) are $b_{1k}(\omega_{\text{ref}})$, $k = r, i$, respectively. The coefficients of $\delta\omega$ in Eqs. (10a) and (10b) and any constant terms follow after expanding $b_{0k}(\omega_{\text{ref}} + \delta\omega)$, $k = r, i$, for small $\delta\omega$.

1. Case 1: $\omega = 0$

First, we note that, by substituting $\omega = 0$ in the second condition of Eqs. (17), we find from Eq. (14b)

$$b_{0i}(\omega_1 = 1) = 0 \tag{19a}$$

$$\Rightarrow L_1 = T_{0\lambda} - (\lambda_b - 1)(\gamma^2 - 1) = 0 \tag{19b}$$

This recovers the condition for the existence of constant solutions in Eq. (16).

The linearization procedure outlined earlier yields the following linear system of equations:

$$B\delta\sigma - A\delta\omega = 0 \tag{20a}$$

$$A\delta\sigma + B\delta\omega = -L_1 \tag{20b}$$

where the constant parameters A and B are defined by

$$A = c_n(\Delta - \lambda_b)/\mu \tag{21a}$$

$$B = T_{0\lambda} + \gamma^2 + 2\lambda_b - 3 \tag{21b}$$

The solutions $\delta\sigma$ and $\delta\omega$ of Eqs. (20) are

$$\delta\sigma = -AL_1/(A^2 + B^2) \tag{22a}$$

$$\delta\omega = -BL_1/(A^2 + B^2) \tag{22b}$$

and the signs of these solutions are given by

$$\text{sign}\{\delta\sigma\} = -\text{sign}\{AL_1\} \tag{23a}$$

$$\text{sign}\{\delta\omega\} = -\text{sign}\{BL_1\} \tag{23b}$$

There are two cases that need to be considered depending on the sign of A:

$$\text{a) } A > 0 \Rightarrow \Delta > \lambda_b \Rightarrow \lambda_s = \lambda_b/\Delta < 1 \text{ (prolate system)} \tag{24a}$$

$$\text{b) } A < 0 \Rightarrow \Delta < \lambda_b \Rightarrow \lambda_s = \lambda_b/\Delta > 1 \text{ (oblate system)} \tag{24b}$$

In case a, we see that the sign of $\delta\sigma$ is opposite to the sign of L_1. Therefore, $\delta\sigma$ is negative (which implies stability) for points *above* the line L_1. In case b, we find that the half-plane of negative σ values lies *below* the line L_1. Thus, the line L_1 is part of the stability boundary.

2. Case 2: $\omega = \lambda_s - 1$

This is the second ω value that satisfies the necessary and sufficient conditions in Eqs. (17). When inserting this value into the second part of Eqs. (17), we find

$$b_{0i}(\omega_1 = \lambda_s) = 0 \tag{25a}$$

$$\Rightarrow L_2 = T_{0\lambda} - (\Delta - 1)(\gamma^2 - \lambda_s^2) = 0 \tag{25b}$$

An interesting alternative form of Eq. (25b) is found by multiplying it by $(1/\lambda_s)^2 = (\Delta/\lambda_b)^2$:

$$\frac{L_2}{\lambda_s^2} = \frac{T_{0\lambda}\Delta^2}{\lambda_b^2} - (\Delta - 1)\left(\frac{\gamma^2\Delta^2}{\lambda_b^2} - 1\right)$$
$$= -\beta^2\Delta^3 + (T_0 + \beta^2)\Delta^2 + \Delta - 1 = 0 \tag{26}$$

When substituting λ_b for Δ in Eq. (26), we find that the result becomes identical to Eq. (C.3) of [1]. This indicates that the envelope of L_2 over the range of parameters Δ is the undamped stability curve in precisely the same manner as is the case for L_1 with respect to the parameter λ_b. Therefore, we can conclude that the line L_2 will never enter the unstable zone of the undamped case. This property is important for the following parametric discussion.

The application of the same linearization procedure to the reference value $\omega = \lambda_s - 1$ leads to the linear system

$$B'\delta\sigma + A\delta\omega = 0 \tag{27a}$$

$$-A\delta\sigma + B'\delta\omega = -\lambda_s L_2 \tag{27b}$$

where the abbreviation B' is defined by

$$B' = T_{0\lambda} + \gamma^2 + \lambda_s(2\lambda_b - 3\lambda_s) \tag{28}$$

The resulting system in Eqs. (27) has the same structure as Eqs. (20) when replacing A by $-A$, B by B', and L_1 by $\lambda_s L_2$. Therefore, the solutions are identical in structure to those in Eqs. (22):

$$\delta\sigma = \lambda_s L_2 A/(A^2 + B'^2) \tag{29a}$$

$$\delta\omega = -\lambda_s L_2 B'/(A^2 + B'^2) \tag{29b}$$

In this second case, the conclusions are opposite to those of the case $\omega = 0$. In the case $A > 0$, the sign of $\delta\sigma$ equals the sign of AL_2 so that σ is negative (implying stability) for points below the line L_2. This means that the prolate system has its stable half-plane below the line L_2. On the other hand, the oblate system has its stable half-plane (with negative σ values) above the line L_2.

C. Summary of Stability Regions

In summary, the lines L_1 and L_2 together define the stability boundaries for the system including damping. When plotting these lines in the $\{\gamma^2, T_{0\lambda}\}$ plane, we can identify the region that corresponds to $\sigma < 0$ for both lines L_1 and L_2. This is illustrated in Figs. 2a and 2b for a prolate and an oblate system, respectively. The open colored triangular regions indicate where the system is asymptotically stable (i.e., when satisfying $\sigma < 0$). For the prolate system in Fig. 2a, the *body* is a fortiori prolate, whereas the body may still be slightly prolate for the oblate system in Fig. 2b. As mentioned earlier, both lines L_1 and L_2 are tangent to the undamped stability curve for

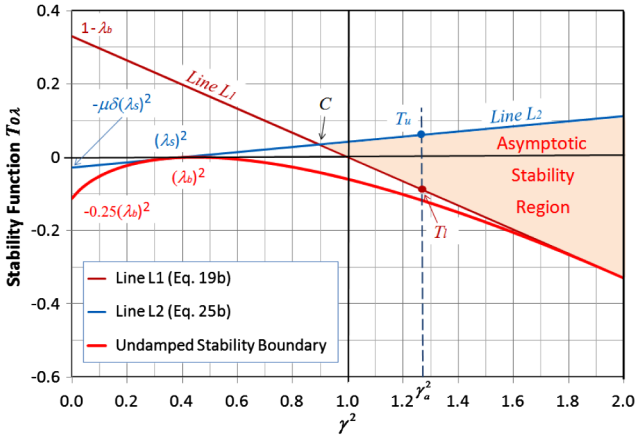

a) Prolate system ($\lambda_s < 1$) with inputs listed in Table 3a

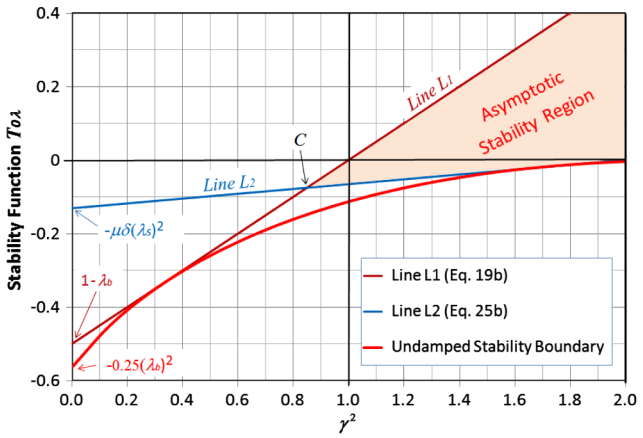

b) Oblate system ($\lambda_s > 1$) with inputs listed in Table 3b

Fig. 2 Illustration of asymptotic stability regions for prolate and oblate systems.

the prolate and oblate configurations. The coefficients of L_1 depend only on λ_b, whereas those of L_2 depend also on the particle mass m.

Table 3 summarizes the relevant physical and derived auxiliary input parameters that have been used in Figs. 2a and 2b, respectively. The definitions of these parameters and their units are listed in Tables 1 and 2. In all cases, the spin rate is taken as $\Omega = 72$ rpm and the particle's vertical coordinate is $l = -1.5$ m.

The point C in Figs. 2a and 2b defines the crossing of the lines L_1 and L_2. It represents the vertex of the asymptotic stability region and has the coordinates

$$\gamma_c^2 = \gamma^2(C) = (1 - \lambda_b + \lambda_s)/\Delta \tag{30a}$$

$$T_{0\lambda c} = T_{0\lambda}(C) = (1-\lambda_b)(1+\lambda_s)(1-\lambda_s/\lambda_b) = \mu\delta(\gamma_c^2 - \lambda_s^2) \tag{30b}$$

Table 3 Physical and auxiliary input parameters

Physical parameters	Values	Auxiliary parameters	Values
Prolate case, Fig. 2a			
M	586.56	μ	0.029774
m	18	λ_b	0.67085
C	377.69	δ	2.3442
A_b	563.0	Δ	1.0698
F	72000	f_n	3.3744
Oblate case, Fig. 2b			
M	325.87	μ	0.029774
m	10	λ_b	1.5
C	500	δ	2.1999
A_b	333.33	Δ	1.0655
F	72000	f_n	5.6993

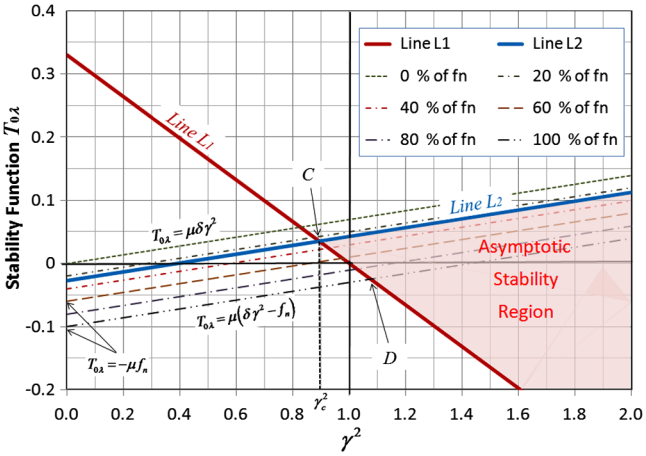

Fig. 3 Stability of prolate system ($\lambda_s < 1$) for different thrust levels.

For an arbitrary value γ_a^2 to the right of point C, we find that the lower and upper bounds of $T_{0\lambda}$ within the triangular stability region correspond to the crossing points of $\gamma^2 = \gamma_a^2$ with the lines L_1 and L_2 (see points T_l and T_u in Fig. 2a). This result will be used in the next section.

In the special case $\lambda_b = \Delta$ we find $\lambda_s = 1$ and $C = A_s$, which implies that all three system inertias are equal. In this case, the lines L_1 and L_2 coincide and the stability region disappears altogether. This confirms that asymptotic stabilization is not possible for a spherical system.

It is surprising that the damping is capable of producing asymptotic stability in the presence of a thrust force for oblate as well as prolate configurations. In the case of a rigid spinner without thrust, the damping is always destabilizing for a prolate system and always stabilizing for an oblate system.

Finally, we mention that the results shown in Fig. 2 are in full agreement with those given by Halsmer and Mingori [3], where the lines L_1 and L_2 correspond to $T_0(q_\Lambda)$ and $T_0(q_\Delta)$, respectively.

V. Interpretation of Stability Results

A. Parametric Interpretations

Because the damping coefficient c does not affect the stability boundaries, the system stability is governed by the remaining eight independent parameters in Table 1. To understand the influence of the mass-spring characteristics $\{m, k\}$, the stability results established earlier will now be interpreted in terms of the parametric representations of the physical inputs μ and k within the $(\gamma^2, T_{0\lambda})$ plane as proposed in Eqs. (33) in [1]. In the present notations, these equations are

$$T_{0\lambda}(\gamma^2; \mu) = \mu(\delta\gamma^2 - f_n) \tag{31a}$$

$$T_{0\lambda}(\gamma^2; k_n) = k_n\{1 - f_n/(\delta\gamma^2)\} \tag{31b}$$

When comparing the linear relationship of $T_{0\lambda}$ as function of γ^2 in Eq. (31a) with the definition of the line L_2 in Eq. (25b), we find that they have equal slopes (because $\Delta - 1 = \mu\delta$). Thus, when considering a given particle mass m, the systems with the corresponding μ (m, M) value correspond to a set of parallel lines within the $\{\gamma^2, T_{0\lambda}\}$ plane. The intercept on the $T_{0\lambda}$ axis equals $-\mu f_n$. The definition of f_n in Table 2 indicates that $f_n > 0$ and increases with the thrust level F and lever arm $|l|$. On the other hand, f_n decreases with the transverse inertia A_b and the square of the spin rate Ω.

B. Prolate Configuration

Figure 3 illustrates the results for a prolate configuration based on the inputs in Table 3. The dotted lines are parallel to line L_2 and represent the constant mass ratio associated with $m = 18$ kg. The upper line represents the no-thrust case $f_n = 0$ and the subsequent lower parallel lines refer to increasing thrust levels up to 100% of the Ulysses injection thrust (i.e., $f_n = 3.3744$).

The thrust level that coincides with the blue line L_2 can be calculated from the equality of Eqs. (25b) and (31a) at the point C ($\gamma^2 = \gamma_c^2$) and its value is $f_{nc} = \delta\lambda_s^2$ (which is 27.3% of the maximum thrust in Fig. 3). Thus, the point C with coordinates $(\gamma_c^2, T_{0\lambda c})$ is associated with this specific thrust level f_{nc}.

Equations (30a) and (30b) show that both γ_c^2 and $T_{0\lambda c}$ are positive for the prolate case. The parameter δ depends only on the body data M, A_b, and lever arm l. In practice, we always have $\lambda_b > \lambda_s$, $\mu\delta$ is small, and Δ is slightly above one. Therefore, $\gamma_c^2 = \omega_{\text{res}}^2/\mu_1$ in Eq. (30a) is slightly below one so that the spring's resonance frequency is below (but close to) the spin rate. These considerations may be summarized as follows (with some margin): So that the system lies within the stable region, it is necessary that the resonance frequency of the spring-mass system is above the spin rate.

When a set of system parameters is given, the actual minimum required value of the spring constant k_c can readily be calculated from

$$k_c = m_{\text{eq}}\Omega^2\gamma_c^2 \tag{32a}$$

$$\text{with} \quad \gamma_c^2 = (1 - \lambda_b + \lambda_s)/\Delta \tag{32b}$$

where $m_{\text{eq}} = m\mu_1 = M\mu$ (see explanation in Sec. II.B).

For any arbitrary γ^2 value to the right of point C, the stability interval for $T_{0\lambda}$ satisfies the conditions

$$(\lambda_b - 1)(\gamma^2 - 1) < T_{0\lambda} < (\Delta - 1)(\gamma^2 - \lambda_s^2) \tag{33}$$

The lower bound becomes negative when $\gamma^2 > 1$ (see also Fig. 3).

The range of thrust values f_n for which $T_{0\lambda}$ remains within the stable region follows from Eq. (33) by substituting the definition of $T_{0\lambda}$ in Table 2:

$$(\lambda_b - 1)(\gamma^2 - 1) < k_n - \mu f_n < (\Delta - 1)(\gamma^2 - \lambda_s^2) \tag{34}$$

After eliminating k_n with the help of the identity $k_n = \mu\delta\gamma^2$ (see Table 2), we obtain:

$$\delta\lambda_s^2 < f_n < \{(\Delta - \lambda_b)\gamma^2 - (1 - \lambda_b)\}/\mu \tag{35}$$

Thus, the *minimum* thrust value f_{nm} for asymptotic stability is independent of the spring constant and is given by

$$f_{nm} = f_{nc} = \delta\lambda_s^2 \tag{36}$$

This minimum value is valid on the line L_2 in Fig. 3 and is the only thrust level for $\gamma^2 = \gamma_c^2$. For the inputs considered here (see Table 3), we find the result $f_{nm} = 0.9218$, which corresponds to the physical force $F_m = A_b\Omega^2 f_{nm}/|l| = 19,669$ N. This result amounts to 27.3% of the Ulysses injection thrust of 72,000 N. For increasing values of γ^2, a range of thrust levels opens up within the stability region in Fig. 3.

The maximum allowable thrust value is a priori given by the right-hand side of the inequality in Eq. (35) and depends, of course, on the spring constant (via γ^2). For illustration, we consider the value $\gamma^2 = 1$, which is slightly larger than γ_c^2. For this value, we find $f_{nM} = \delta = 2.3442$ or $F_M = 50,018$ N, which is 69.5% of the Ulysses injection thrust (see also Fig. 3). Vice versa, a given thrust level requires a minimum value of the spring constant. For instance, when considering the actual Ulysses thrust level of $f_n = 3.3744$, the minimum required value for γ^2 can be calculated from Eq. (35):

$$\gamma_{\min}^2 = \frac{1 - \lambda_b + \mu f_n}{1 - \lambda_b + \mu\delta} \tag{37}$$

which gives $\gamma_{\min}^2 = 1.0769$ (i.e., point D in Fig. 3). This result confirms that the normalized resonance frequency $\omega_{\text{res}} = 1.0222$ is just above one.

Next, we focus on the characteristics of the roots. Numerical calculations indicate that root 1 has $|\omega| \approx 2$ with a real part that is always negative. Roots 2 and 3 have imaginary parts, which are the continuations of the nutation frequency and zero frequency, respectively. Their real parts are fairly small and may be positive or negative.

Figure 4a shows the real parts of roots 2 and 3 as functions of the thrust level f_n while traversing the stable region in Fig. 3 along the vertical line $\gamma^2 = 1.237$. Figure 4b shows the corresponding complex roots. The σ's of roots 2 and 3 are negative only *inside* the stable region. The σ value of root 2 goes from positive to negative when entering the stable region from above (i.e., the line L2 in Fig. 3 and the curves associated with root # 2 in Figs. 4a and 4b). The real part of root 3 is already negative when entering the stable region from above. Subsequently, it moves "along the curves associated with root # 3 in the direction of the arrows in Figs. 4a and 4b. Finally, it crosses the stability boundary $\sigma = 0$ at $f_n = 5.520$ in Fig. 4a, while crossing line L_1 in Fig. 3 from above (on the vertical line $\gamma^2 = 1.237$).

The negative real parts of roots 2 and 3 become equal when $f_n = 4.189$ in Figs. 4a and 4b (i.e. at the value $\sigma_{\text{eq}} = -0.001312$). Because $|\sigma|$ is the inverse of the time constant of an exponential decay, it will take $3/|\sigma_{\text{eq}}|$ spin periods to reduce a nutation disturbance to 5% of its initial value during thrusting. This number of spin periods contains more nutation periods than the periods of the low frequency (i.e., root 3). A priori, the point where these two negative σ values become equal may be interpreted as having "maximum" stability. However, the impacts of the two roots on the nutation damping may be very different and should be taken into account.

The damping coefficient $c_n = 10^{-3}$ gives $3/|\sigma_{\text{eq}}| = 2286$ spin periods or 38 min at 60 rpm. The larger damping $c_n = 10^{-2}$ leads to $f_n = 4.174$, $\sigma_{\text{eq}} = -0.01278$, and only 3.9 min at 60 rpm.

C. Oblate Configuration

The stability region of the oblate configuration is shown in Fig. 5 with inputs specified in Table 3, which were also used in Fig. 2b. The slope of line L_1 is now positive and corresponds to the upper

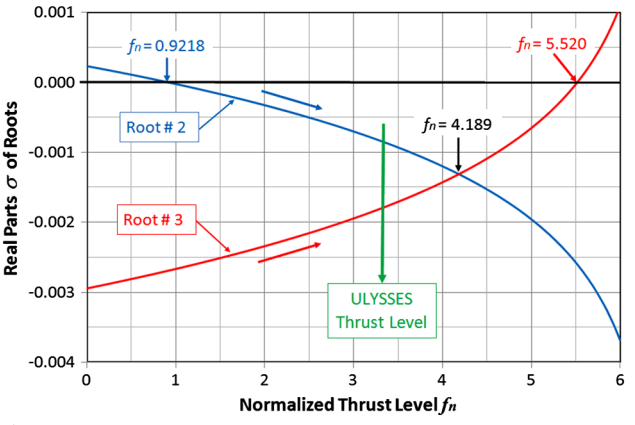

a)

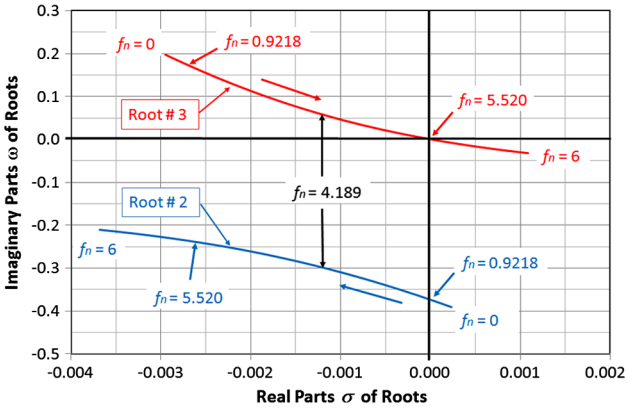

b)

Fig. 4 Prolate system (inputs in Table 3; $c_n = 10^{-3}$): a) real parts of roots vs thrust; b) complex roots.

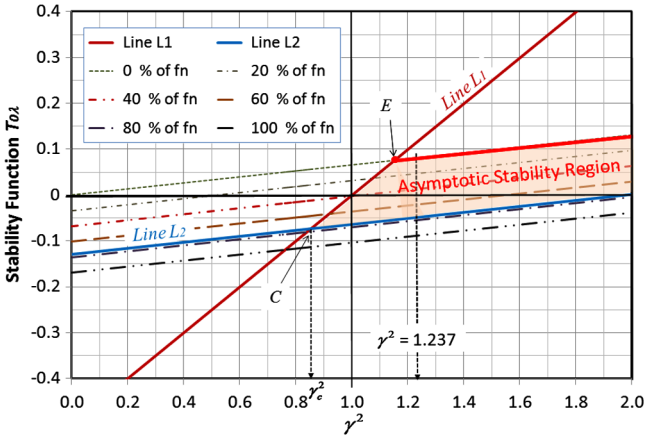

Fig. 5 Stability of oblate system ($\lambda_s > 1$) for different thrust levels.

boundary of the stability zone. It is clear from Eqs. (30a) and (30b) and from Figs. 2b and 5 that $\gamma_c^2 < 1$ and $T_{0\lambda c} < 0$ for the oblate system.

The two inequalities in Eq. (35) swap sides because L_1 is now the upper stability boundary of $T_{0\lambda}$ and L_2 is the lower boundary. Therefore, the limit $\delta\lambda_s^2$, which is independent of the spring constant, is the maximum allowed thrust value for stability in this case. This limit corresponds to the 76.5% thrust line in Fig. 5. The minimum physically possible value of the thrust level is zero. This constraint changes the open triangle to a zone bounded by two parallel lines and a segment of the line L_1. The lower limit $\gamma_{\min}^2$ for the spring constant that stabilizes the system for zero thrust and for the given particle mass follows from Eq. (35):

$$\gamma_{\min}^2 = \frac{1-\lambda_b}{1-\lambda_b+\mu\delta} \tag{38}$$

This coordinate corresponds to point E (with $\gamma_E^2 = 1.1507$) in Fig. 5 and makes the shape of the stability region become trapezoidal.

Figure 6a shows the real parts of the roots 2 and 3 as functions of the thrust f_n for an oblate body with inertia ratio $\lambda_b = 1.5$. The inputs are given in Table 3 and are the same as used in Fig. 5. The results indicate that the stable range (i.e., $\sigma < 0$) stretches up to $f_n = 4.360$ (i.e., 76.5% of the maximum thrust in the oblate case) where the real part of root 3 vanishes. In the absence of thrust, the system is stable because both σ values are negative in Fig. 6a.

Figures 6a and 6b show that the damping of root 2 (which is now the continuation of the constant solution) increases for larger thrust levels. Root 3 (i.e., the continuation of the nutation frequency) provides strong damping in the absence of thrust but the damping diminishes as the thrust increases and eventually leads to instability when $f_n > 4.360$. Also, in the oblate case, the root 1 (not shown) with $|\omega| \approx 2$ always has a negative real part.

D. Application to Ulysses with Low Particle Mass Ratio

In the previous sections, the thrust was considered a variable parameter, whereas the stability zone was traversed along a vertical line of constant γ^2 value. Here, we consider the case in which the prolate Ulysses configuration in Figs. 2a and 3 will be stabilized by a particle with mass ratio μ of, at most, 1% (i.e., $m < 5.925$ kg) for the full-thrust case. Apart from m and μ, the other inputs specified in Table 3 remain valid here.

Figure 7 shows the two stability boundary lines L_1 and L_2 as well as the point D, which is the vertex of the stability region. The point B corresponds to the location at which $T_{0\lambda}$ vanishes. Equation (31a) gives $\gamma_B^2 = f_n/\delta = F/(M\Omega^2|l|)$. Consequently, the lines of constant positive μ values have $T_{0\lambda} < 0$ for $\gamma^2 < \gamma_B^2$ and $T_{0\lambda} > 0$ for $\gamma^2 > \gamma_B^2$. At the 100% Ulysses thrust level, we have $\gamma_B^2 = 1.435 > 1$ and the parts of the stability region where $T_{0\lambda}$ is positive (negative) to the left (right) of γ_B^2 are eliminated for positive μ values. The full-thrust $\mu = 1\%$ line enters the stability triangle at point D and stabilization is possible for $\gamma^2 > \gamma_D^2 = 1.029$. The coordinate γ_D^2 corresponds to $k_n = 0.02413$ or $k = A_b(\Omega^2/l^2)k_n = 343.2$ N/m.

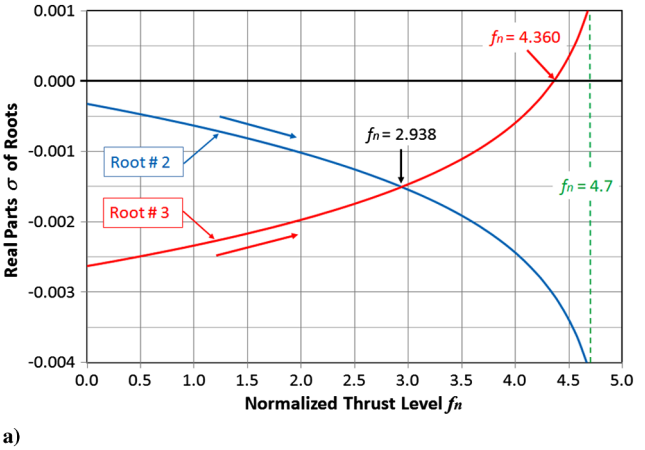

a)

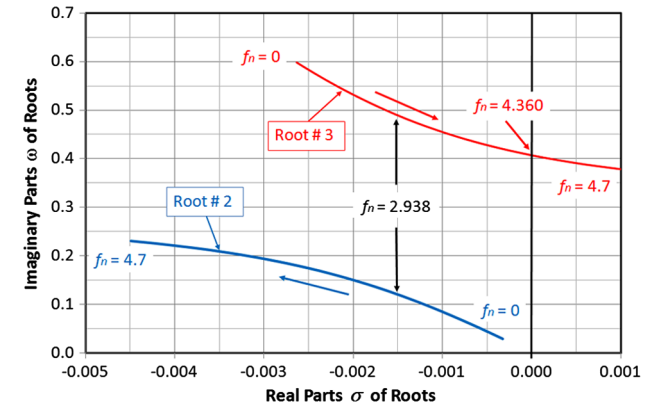

b)

Fig. 6 Oblate system (inputs in Table 3; $c_n = 10^{-3}$): a) real parts of roots vs thrust; b) complex roots.

The two small colored triangles in Fig. 7 are the remainders of the original open triangular region (shown in Fig. 3), where asymptotic stability is possible for mass ratios μ below 1% under the assumed inputs for this case.

Figure 8 shows the real parts of the roots 2 and 3 as a function of γ^2. The line associated with root 2, which is the continuation of the zero solution. It becomes negative when γ^2 exceeds 1.029 and decreases gradually for increasing γ^2. The damping for root 3 (i.e., the perturbed nutation frequency) is also shown in Fig. 8. The value of σ is already negative when entering the stability region but keeps increasing monotonically for larger stiffness values. The damping produced by the frequency of root 1 is systematically an order of magnitude larger (not shown).

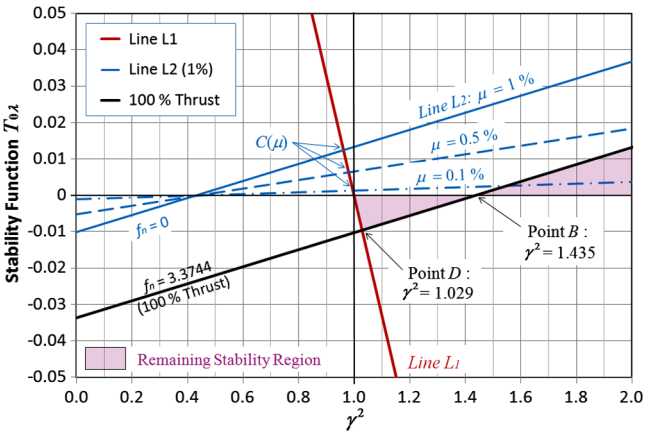

Fig. 7 Stabilization of prolate Ulysses system for $\mu \leq 0.01$.

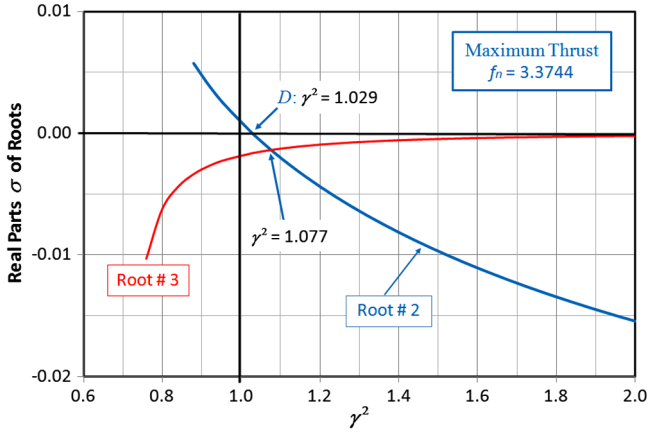

Fig. 8 Real parts of roots 2 and 3 for Ulysses system ($\mu = 0.01$; $c_n = 10^{-3}$).

VI. Conclusions

The effectiveness of a damped mass-spring system on a spinning satellite under axial thrust is investigated in detail by using Lyapunov's first method. It is found that the transition from asymptotically stable to unstable can occur for only two values of the system frequency. This allows calculating the asymptotic stability boundaries by a standard linearization procedure of a system of two equations with real coefficients, which is equivalent to the system's characteristic equation. Analyses and simulations confirm that both prolate and oblate spinners can be stabilized by such a system. Valuable new visualizations and interpretations are established in terms of the adaptation of the familiar maximum-axis rule to a spinner under axial thrust. First of all, an oblate spinner under axial thrust may be destabilized by the damping system considered here. A new result is that this happens in any case if the thrust exceeds a certain threshold level. In the case of a prolate spinner, for which damping is always destabilizing in the absence of thrust, ranges for the values of the mass and spring constant exist where the system can be stabilized under axial thrust. A numerical example based on the Ulysses injection parameters indicates that it is not obvious that a nutation damper consisting of such a damped mass-spring system would be suitable for applications in which the damping time is limited. Finally, it may be of interest to investigate whether similar results for the damping capabilities under axial thrust also apply to more common nutation dampers such as fluid-in-ring or fluid-in-tube systems.

Appendix A: First Integral for the Undamped Case

A1 System of Equations

The system of equations in real form is given in Eqs. (2). In the absence of damping (i.e., when $c_n = 0$) this system can be simplified as follows:

$$\omega_1' + (\lambda_b - 1)\omega_2 + T_{0\lambda}x_2/l = 0 \tag{A1a}$$

$$\omega_2' - (\lambda_b - 1)\omega_1 - T_{0\lambda}x_1/l = 0 \tag{A1b}$$

$$x_1'' - 2x_2' + (T_{0\lambda} + \gamma^2 - 1)x_1 + \lambda_b l\omega_1 = 0 \tag{A1c}$$

$$x_2'' + 2x_1' + (T_{0\lambda} + \gamma^2 - 1)x_2 + \lambda_b l\omega_2 = 0 \tag{A1d}$$

We introduce the state vector $\boldsymbol{x} = (\omega_1, x_1, v_2, \omega_2, x_2, v_1)^T$ with $v_1 = -x_1'$ and $v_2 = x_2'$. Next, we express Eqs. (A1) in the form $\boldsymbol{x}' = A\boldsymbol{x}$ with the 6×6 matrix A defined by

$$A = \begin{bmatrix} O & -A_1 \\ A_1 & O \end{bmatrix} \tag{A2a}$$

$$\text{with} \quad A_1 = \begin{bmatrix} \lambda_b - 1 & T_{0\lambda}/l & 0 \\ 0 & 0 & 1 \\ l\lambda_b & T_{0\lambda} + \gamma^2 - 1 & -2 \end{bmatrix} \tag{A2b}$$

The state vector $\boldsymbol{x}$ adopted here is similar to the one used in Eq. (20) of Halsmer et al. [3] except for the different sign of v_1, which is needed for establishing the structure of the matrix A in Eqs. (A2).

A2 Construction of First Integral

Equations (A1) are convenient for building a first integral. First, we multiply each of Eqs. (A1a) and (A1b), which are normalized by the spin rate, with its corresponding $\omega_i (i = 1, 2)$ and add the results:

$$\frac{1}{2}\frac{\mathrm{d}}{\mathrm{d}\tau}(\omega_1^2 + \omega_2^2) = \frac{T_{0\lambda}}{l}(x_1\omega_2 - x_2\omega_1) \tag{A3}$$

Similarly, after multiplying the equations for x_i in Eqs. (A1c) and (A1d) with its corresponding $x_i' (i = 1, 2)$ and adding the results, we find:

$$\frac{1}{2}\frac{\mathrm{d}}{\mathrm{d}\tau}\{(x_1'^2 + x_2'^2) + (T_{0\lambda} + \gamma^2 - 1)(x_1^2 + x_2^2)\} = -l\lambda_b(x_1'\omega_1 + x_2'\omega_2) \tag{A4}$$

Next, we multiply each equation for $\omega_i (i = 1, 2)$ in Eqs. (A1a) and (A1b) with its corresponding x_i (for $i = 1, 2$) and add the results:

$$x_1\omega_1' + x_2\omega_2' = -(\lambda_b - 1)(x_1\omega_2 - x_2\omega_1) \tag{A5}$$

Then we eliminate the term $(x_1\omega_2 - x_2\omega_1)$ on the right-hand side of Eq. (A3) with the help of Eq. (A5) and find:

$$\frac{1}{2}\frac{\mathrm{d}}{\mathrm{d}\tau}(\omega_1^2 + \omega_2^2) = -\frac{T_{0\lambda}}{l(\lambda_b - 1)}(x_1\omega_1' + x_2\omega_2') \tag{A6}$$

Finally, we multiply both sides of Eq. (A4) by the constant term $T_{0\lambda}/\{l^2\lambda_b(\lambda_b - 1)\}$:

$$\frac{1}{2}\frac{T_{0\lambda}}{l^2\lambda_b(\lambda_b - 1)}\frac{\mathrm{d}}{\mathrm{d}\tau}\{(x_1'^2 + x_2'^2) + (T_{0\lambda} + \gamma^2 - 1)(x_1^2 + x_2^2)\} = -\frac{T_{0\lambda}}{l(\lambda_b - 1)}(x_1'\omega_1 + x_2'\omega_2) \tag{A7}$$

The bracketed terms on the right-hand sides of Eqs. (A6) and (A7) can be combined into the derivative of $(x_1\omega_1 + x_2\omega_2)$. Furthermore, the derivative terms on the left-hand sides of Eqs. (A6) and (A7) can be merged, and so we find, by adding Eqs (A6) and (A7):

$$\frac{1}{2}\frac{\mathrm{d}}{\mathrm{d}\tau}\left\{\omega_1^2 + \omega_2^2 + \frac{T_{0\lambda}}{l^2\lambda_b(\lambda_b - 1)}[(x_1'^2 + x_2'^2) + (T_{0\lambda} + \gamma^2 - 1)(x_1^2 + x_2^2)]\right\} = -\frac{T_{0\lambda}}{l(\lambda_b - 1)}\frac{\mathrm{d}}{\mathrm{d}\tau}(x_1\omega_1 + x_2\omega_2) \tag{A8}$$

Equation (A8) is equivalent to the total differential $\mathrm{d}V = 0$ with corresponding first integral V:

$$V = \omega_1^2 + \omega_2^2 + \frac{T_{0\lambda}}{l^2\lambda_b(\lambda_b - 1)}\{x_1'^2 + x_2'^2 + (T_{0\lambda} + \gamma^2 - 1)(x_1^2 + x_2^2)\} + \frac{2T_{0\lambda}}{l(\lambda_b - 1)}(x_1\omega_1 + x_2\omega_2) \tag{A9}$$

V is a quadratic function of the state vector $\boldsymbol{x}$ (i.e. $V = x^T Bx$), with the matrix B defined by:

$$B = \begin{bmatrix} B_1 & O \\ O & B_1 \end{bmatrix} \quad \text{with} \quad B_1 = \frac{1}{l^2\lambda_b} \begin{bmatrix} l^2\lambda_b & l\lambda_b c_3 & 0 \\ l\lambda_b c_3 & c_2 c_3 & 0 \\ 0 & 0 & c_3 \end{bmatrix} \tag{A10}$$

The matrix B and its elements have the following properties and definitions:

$$B = B^T \tag{A11a}$$

$$B_1 = B_1^T \tag{A11b}$$

$$c_2 = T_{0\lambda} + \gamma^2 - 1 \tag{A11c}$$

$$c_3 = T_{0\lambda}/(\lambda_b - 1) \tag{A11d}$$

If B were a positive-definite matrix, then the first integral V in Eq. (A9) would be a Lyapunov function. Furthermore, because the derivative of V along a solution trajectory is zero (i.e., $V' < 0$) by design, we have a sufficient condition for oscillatory stability. (Note, only when $V' < 0$ do we have a necessary and sufficient condition for asymptotic stability). So that the matrix B_1 is positive definite, it is necessary and sufficient (according to Sylvester's criterion) that all of its three leading principal minors are positive. This leads to the following two nontrivial conditions:

$$\frac{c_3}{l^2}\left(\frac{c_2}{\lambda_b} - c_3\right) > 0 \tag{A12a}$$

$$\frac{c_3^2}{l^4\lambda_b}\left(\frac{c_2}{\lambda_b} - c_3\right) > 0 \tag{A12b}$$

The positive l^2 and l^4 terms may be dropped so that Eqs. (A12a) and (A12b) yield the following conditions:

$$\text{a)}\ c_2 > \lambda_b c_3 \Rightarrow T_{0\lambda} + \gamma^2 - 1 > \lambda_b T_{0\lambda}/(\lambda_b - 1) \tag{A13a}$$

$$\text{b)}\ c_3 > 0 \Rightarrow T_{0\lambda}/(\lambda_b - 1) > 0 \tag{A13b}$$

Here, the different signs of $\lambda_b - 1$ need to be distinguished because it is negative for a prolate body and positive for an oblate body. For the prolate body (i.e., $0 < \lambda_b < 1$), Eqs. (A13a) and (A13b) produce

$$T_{0\lambda} > (\lambda_b - 1)(\gamma^2 - 1) \tag{A14a}$$

$$\text{and} \quad T_{0\lambda} < 0 \tag{A14b}$$

The first condition states that the region of oscillatory stability (see [1]) is above the line L_1, which is consistent with the results shown in Figs. 2a and 3. The second condition, however, limits the region to negative values of $T_{0\lambda}$ so that the remaining area covers only part of the oscillatory stable region of the $\{T_{0\lambda}, \gamma^2\}$ plane.

It can be confirmed that similar conditions as in Eqs. (A14a) and (A14b) also hold for an oblate satellite body (i.e., $1 < \lambda_b < 2$) except that the two inequality signs will be inverted. The comparison with the results in Fig. 2b shows that, also for the oblate case, the resulting region covers only part of the stability region.

These results confirm that the stability results obtained from a Lyapunov function are sufficient (see Müller [8]) and depend on the particular Lyapunov function that is being used. Although the first integral found here is constructed in a similar way as an energy integral, it is not the total energy of the system.

Appendix B: First Integral with Change of Variables

Now the variables ω_i are replaced by $w_i = \omega_i l\,(i = 1, 2)$ and x_1', x_2' are replaced by

$$v_{b1} = x_2 - w_2 - x_1' \tag{B1a}$$

$$v_{b2} = x_1 - w_1 + x_2' \tag{B1b}$$

where $v_{bi}(i = 1, 2)$ is the particle's velocity in the body frame when the rotation of the body with reference point O_b is taken into account. The new variables $w_i = \omega_i l$ (for $i = 1, 2$) are linear velocities. Because the independent variable τ is nondimensional, the velocities Ωx_i $(i = 1, 2)$ appear to have the dimension of distance.

In terms of the new variables $\boldsymbol{x}_n = (w_1, x_1, \nu_{b2}, w_2, x_2, \nu_{b1})^T$ the system of Eqs. (A1) becomes

$$w_1' = -(\lambda_b - 1)w_2 - T_{0\lambda}x_2 \tag{B2a}$$

$$w_2' = (\lambda_b - 1)w_1 + T_{0\lambda}x_1 \tag{B2b}$$

$$x_1' = -w_2 + x_2 - v_{b1} \tag{B2c}$$

$$x_2' = w_1 - x_1 + v_{b2} \tag{B2d}$$

$$v_{b1}' = -v_{b2} + \gamma^2 x_1 \tag{B2e}$$

$$v_{b2}' = v_{b1} - \gamma^2 x_2 \tag{B2f}$$

When writing Eqs. (B2) in matrix form (i.e., $\boldsymbol{x}_n' = A_{nxn}$), we find that the matrix structure of A_n is identical to the one in Eq. (A2a):

$$A_n = \begin{bmatrix} O & -A_{1n} \\ A_{1n} & O \end{bmatrix} \tag{B3a}$$

$$\text{with} \quad A_{1n} = \begin{bmatrix} \lambda_b - 1 & T_{0\lambda} & 0 \\ 1 & -1 & 1 \\ 0 & -\gamma^2 & 1 \end{bmatrix} \tag{B3b}$$

The first integral for the new system in Eqs. (B2) can now easily be obtained from

$$w_1 w_1' + w_2 w_2' = -T_{0\lambda}(x_2 w_1 - x_1 w_2) \tag{B4a}$$

$$x_1 x_1' + x_2' x_2' = (x_2 w_1 - x_1 w_2) - (x_1 v_{b1} - x_1 v_{b2}) \tag{B4b}$$

$$v_{b1} v_{b1}' + v_{b2} v_{b2}' = \gamma^2(x_1 v_{b1} - x_2 v_{b2}) \tag{B4c}$$

When adding the terms of Eqs. (B4) with respective coefficients $\{1, T_{0\lambda}, T_{0\lambda}/\gamma^2\}$ we obtain the new total differential V_n. Thus, the first integral in terms of the new state vector $\boldsymbol{x}_n$ is

$$V_n = w_1^2 + w_2^2 + T_{0\lambda}(x_1^2 + x_2^2) + \frac{T_{0\lambda}}{\gamma^2}(v_{b1}^2 + v_{b2}^2) \tag{B5}$$

This result is a quadratic form on a *diagonal* matrix, which is positive definite when $T_{0\lambda} > 0$ (from Sylvester's criterion). By construction, we have $V_n' = 0$. Therefore, in terms of this new state vector, it is clear that the first integral V_n is indeed a Lyapunov

function. This also confirms that the system is oscillatory stable when $T_{02} > 0$.

Again, this sufficient condition does not produce the total oscillatory stable region for the undamped case (see [1]). In Halsmer and Mingori [3], a Lyapunov function with $V' < 0$ has been constructed for the system including damping. When this Lyapunov function is positive definite, we have a necessary and sufficient condition for asymptotic stability and the results are in full agreement with the Lyapunov direct method used in this paper.

References

[1] Janssens, F. L., and van der Ha, J. C., "Stability of Spinning Satellite Under Axial Thrust and Internal Mass Motion," *Acta Astronautica*, Vol. 94, No. 1, Jan. 2014, pp. 502–514. doi:10.1016/j.actaastro.2012.09.013

[2] Mingori, D. L., and Yam, Y., "Nutational Stability of a Spinning Spacecraft with Internal Mass Motion and Axial Thrust," *AIAA/AAS Astrodynamics Conference*, AIAA Paper 1986-2271, Aug. 1986.

[3] Halsmer, D. M., and Mingori, D. L., "Nutational Stability and Passive Control of Spinning Rockets with Internal Mass Motion," *Journal of Guidance, Control, and Dynamics*, Vol. 18, No. 5, 1995, pp. 1197–1203. doi:10.2514/3.21525

[4] Yam, Y., Mingori, D. L., and Halsmer, D. M., "Stability of a Spinning Axisymmetric Rocket with Dissipative Internal Mass Motion," *Journal of Guidance, Control, and Dynamics*, Vol. 20, No. 2, 1997, pp. 306–312. doi:10.2514/2.4038

[5] Hughes, P. C., "Spacecraft Attitude Dynamics," Dover, New York, 2004, pp. 480–521.

[6] Gantmacher, F. R., "Theory of Matrices," *American Mathematical Society*, Vol. II, Providence, RI, 2000, pp. 248–249.

[7] Lang, A., and Halsmer, D., "Constrained Optimization of Passive Coning Attenuators for Spinning Spacecraft Under Thrust," *Advances in the Astronautical Sciences*, Vol. 108, No. 2, 2001, pp. 155–162.

[8] Müller, P. C., *Stabilität und Matrizen*, Springer, Berlin, 1977, p. 78.